THE ASTRONOMICAL JOURNAL VOLUME 92, NUMBER 5 NOVEMBER 1986

# THE AMORPHOUS GALAXY NGC 3448. I. PHOTOMETRY, DYNAMICS, AND MODELING

LOUIS NOREAU[a] AND P. P. KRONBERG
Department of Astronomy, University of Toronto, 60 St. George Street, Toronto, Ontario, M5S 1A7, Canada
*Received 10 April 1986; revised 17 July 1986*

## ABSTRACT

To further our knowledge of the relatively rare amorphous type galaxies, we launched a detailed study of NGC 3448 in the Arp 205 interacting system. This first paper of a series of two discusses the optical and H I morphology and dynamics, and modeling of the galaxy. $B$, $V$, and $R$ images were secured with the CCD camera at the 0.9 m telescope at KPNO. Color index maps were produced. A striking variation in color indices is visible across the face of the galaxy. The $\langle B-V \rangle$ of the southern half is similar to that of the arms of the latest-type spirals. The redder regions in the north, and east of the center, are probably obscured by foreground material. We used the VLA to perform a complete synthesis of the 21 cm line emission, and were able to separate the H I emission of NGC 3448 from that of its dwarf companion UGC 6016. Although the latter is interacting with NGC 3448, it has remarkably regular dynamics, and its hydrogen distribution is similar to that of other galaxies of the same type. By contrast, the H I morphology of NGC 3448 is quite perturbed due to the tidal interaction with UGC 6016. We have produced a successful dynamic model of the Arp 205 interacting system. It satisfactorily reproduces most of the large-scale features of NGC 3448, and shows that the shape and dynamics of the galaxy are consistent with a tidal interaction. Tidal material appears to be reintegrating with the galaxy, and also causes the obscuration observed in the optical region. We believe we have reached a consistent overall understanding of this galaxy system.

## I. INTRODUCTION

### *a) The NGC 3448/Arp 205 System*

Of the galaxies found in the amorphous class, only M82 has been the focus of much attention. After M82 and NGC 3077 (also a member of the M81 group of galaxies), NGC 3448 is the nearest amorphous galaxy which can easily be reached from the northern hemisphere observatories.

A faint dwarf companion, UGC 6016, lies south-preceding and is classified by de Vaucouleurs *et al.* (1976) (hereafter referred to as RC2) as SB(s)d. NGC 3448 and UGC 6016 are together listed as entry #205 in the *Atlas of Peculiar Galaxies* (Arp 1966). Herein Arp 205 will refer to the pair consisting of both galaxies.

Larson and Tinsley (1979) found that "Arp 205" was one of the bluest galaxies (corrected colors) in Arp's (1966) atlas, suggesting that NGC 3448 is among the galaxies with the highest star-formation rate per unit mass. This agrees with the requirement of formation of new stars in the amorphous galaxies.

A corrected Harvard magnitude of $m_c = 12.03$ is given by the RC2 for NGC 3448, and a face-on corrected magnitude of $B_T^0 = 11.59$. UGC 6016 has a Zwicky magnitude evaluated from the POSS plate copy by Nilson of 17 $m_{pg}$. After reduction to the $B_T$ system according to the method of de Vaucouleurs and Pence (1979), and corrections for external and internal absorption, $B_T^0 = 14.8$ is derived.

De Vaucouleurs (1979) assigns NGC 3448 to the Ursa Major I(X) group. However, Huchra and Geller (1978), with Turner and Gott (1976), do not include it in any group of galaxies. This reflects both the looseness and proximity of the group. The galaxy lies in the local supercluster plane, in the Canes Venatici cloud (Tully 1982). The distance to NGC 3448 cannot be easily assessed due to its unique properties. Previous detailed studies (Bottinelli *et al.* 1978; Reakes 1979; and Bertola *et al.* 1984) used de Vaucouleurs' (1975) distance to the UMa I (X) group, 10.7 Mpc, which we also have adopted even though it is quite uncertain.

Bottinelli *et al.* (1978) made a detailed study of NGC 3448 and reported a "double velocity profile" for the inner part of NGC 3448 for which they proposed two possible explanations: either NGC 3448 has a nonsymmetrical rotation curve and strong absorption in its central region or it is a double interacting galaxy with two different rotation systems. They did not elaborate on the possible tidal encounter with UGC 6016.

Reakes (1979) published synthesis maps of NGC 3448 at the 21 cm line with the Cambridge Half-Mile synthesis radio telescope, but did not detect the double velocity profile. He established the sense of rotation of UGC 6016 and reported a relatively high mass for the dwarf. This led him to suggest that NGC 3448 and UGC 6016 might have experienced a near coplanar parabolic encounter at a distance from 10 to 15 kpc about 400 to 800 million years ago.

More recently, Bertola *et al.* (1984) presented matched H I and optical velocity curves of NGC 3448 (a combined version of these curves can be found in Noreau 1985). They reported a "hump" in both velocity curves which could be identified with the double velocity feature reported by Bottinelli *et al.* (1978). They concluded that the "hump cloud" caused the obscuration observed in the NE of the galaxy and probably originated from tidal interaction. They ruled out the hypothesis of a double interacting system proposed by Bottinelli *et al.* (1978). They also presented a UV spectrum of the nuclear region, which revealed the presence of a hot nuclear component.

### *b) The Amorphous Galaxies*

The class of amorphous galaxies was introduced by Sandage and Brucato (1974) to replace the Irr IIs, as it was realized that new stars were being formed in them and that the name was not indicative of the stellar content. Only the most disturbed Irr IIs were reclassified as amorphous for a total of 14: NGC 520, 625, 1510, 1531, 1705, 1800, 2968,

---

[a] Present address: Département de physique, Université Laval, Québec City, Québec G1K 7P4, Canada.

 0004-6256/86/051048-20$00.90  

3034 (M82), 3077, 3125, 3448, 4694, 5253, and 6835 (Sandage and Brucato 1974; Sandage and Tammann 1981; Eichendorf and Nieto 1984). The classification criteria are: an "amorphous appearance to the unresolved light, sometimes with embedded resolved stars, but sometimes not as in M82, NGC 3077, and NGC 3448," no spiral structure should be evident, and superposed irregular dust lanes might be present. The members of the new class share also similar photometric and spectroscopic properties: their mean corrected colors are $\langle B-V\rangle \simeq 0.6$, $\langle U-B\rangle \simeq -0.1$ but with an appreciable scatter. Sandage and Brucato (1979) add: "the strong underlying A star absorption spectrum for the amorphous galaxies, together with their characteristic hot, young stars, emission spectrum, and their color, all show the presence of a newly formed population in the amorphous class as well as in the Irr I types." Generally, this emission is spread throughout the disk.

The archetype amorphous galaxy is M82. The activity observed in its central regions is characterized by strong far-infrared emission (Telesco and Harper 1980 and references therein), CO emission line (Rickard *et al.* 1975), the presence of numerous SN and SNR (Kronberg, Biermann, and Schwab 1985 and references therein), and is presumed to be due to the burst of star formation caused by compression of infalling gas previously stripped from M82 by tidal interaction with a member of the M81 group (O'Connell and Mangano 1978; Cottrell 1977; Gottesman and Weliachew 1977; Killian and Gottesman 1979).

Gottesman and Weliachew (1977) and Cottrell (1978) suggested that the Irr IIs were normal galaxies which have received an injection of fresh gas triggering active star formation from galaxy-galaxy interaction. Their relative scarcity ($\sim 1\%$), and presence in small groups of galaxies, strongly argue for this.

Section II presents the optical and radio observations of NGC 3448 together with the reduction procedures. The main results are discussed in Sec. III, Sec. IV discusses a model of the interaction, and Sec. V summarizes our conclusions on the nature of NGC 3448. A coming paper (Noreau and Kronberg 1986) will discuss the continuum radio emission from the center.

## II. OBSERVATIONS AND DATA REDUCTION

### *a) Optical Data*

Arp 205 was observed on 21 and 23 January 1983 at Kitt Peak National Observatory* with the #1 0.9 m telescope equipped at the $f/7.5$ focus with the CCD direct-imaging camera, the "Gold autoguider," and a filter wheel with a set of Johnson-Cousins *UBVRI* filters (Goad 1981; Schoening 1983; McGuire 1983). The field of the CCD was 7'.3 (E-W) by 4'.6 (N-S). One $R$, one $V$, and two $B$ images were secured despite less than ideal weather conditions.

The standard initial processing of the image (McGuire 1983; Djorgovski 1984) was performed on the interactive picture processing system (IPPS) at the KPNO headquarters in Tucson. The analysis was completed using the NRAO AIPS station in the Department of Astronomy in Toronto.

After transposing the CCD image to the proper sky orientation, the "frame" positions of eight secondary-standard stars on every CCD image were found by fitting a parabola to their peak intensity. The PDS microdensitometer of the David Dunlap Observatory was used to measure positions of these eight secondary standards with respect to 19 stars listed in the *Smithsonian Astrophysical Observatory Star Catalogue* (1966, SAO) on a plate copy of the Palomar Observatory Sky Survey O plate. The B1950.0 positions of these eight secondary standards were derived by fitting a high-order polynomial (with cross terms) with an internal consistency of about 0''.1. Finally the B1950.0 sky position of the center of the CCD grid was calculated using a least-squares fitting routine.

Since the CCD images contained no night-sky fringing and any apparent large-scale variations of the sky level across the CCD image were to less than the noise level, only a constant value needed to be subtracted from every map to eliminate the sky foreground.

The atmospheric conditions did not permit direct photoelectric calibration. We did, however, calibrate the images in the natural system of the CCD camera and the filters by using the calibrated aperture $B$ and $V$ magnitudes of NGC 3448 from the catalog of Longo and de Vaucouleurs (1983). For our pseudoaperture photometry calibration, a weighted flux average at the four largest apertures listed by Longo and de Vaucouleurs (1983) was used: $B = 12.55$ and $V = 12.08$ with a nominal aperture diameter of 2'.5. Unfortunately, no values were found for the $R$ magnitude in the literature. However, an $R$ magnitude image was produced without a calibration for the zero point; an assumed integrated value of $R = 11$ was assigned to the galaxy. The images were transformed into mag arcsec$^{-2}$. A formal transformation with color terms to the Johnson system for the $B$ and $V$ images was not made because of the lower quality of the $V$ image. However, the resulting images should not be very different from Johnson's magnitudes since for the $B$ and $V$ magnitudes the color term at KPNO is quite small (Borra *et al.* 1985; Sydserff and Cruise 1983). Contour maps of one of the $B$ images are displayed in Fig. 1. Table I lists some characteristics of the images.

The galactic extinction estimates of Burstein and Heiles (1984) in the direction of NGC 3448 indicate that no reddening corrections are necessary before building color-index maps. The best $B$ image was displaced to the coordinates of the $V$ image, and a subtraction was performed to get the $B-V$ map. For the $B-V$ map, the color correction was carried out.

Only the pixels brighter than 21 mag arcsec$^{-2}$ in the $V$ magnitude picture were used to compute the color-index map in order to keep the error to less than 0.1 mag arcsec$^{-2}$ in the regions of low intensity. The $B-V$ map is displayed in Fig. 2(a). An uncalibrated $B-R$ map [Fig. 2(b)] was also produced.

### *b) H I Line*

Arp 205 was observed with the Very Large Array (VLA)† in the C, or 3 km, configuration using the spectral-line system. Information concerning line observing techniques and data processing can be found in D'Addario (1982), Rots (1982), van Gorkom (1982), Ekers and van Gorkom (1983), and Rots (1983).

We chose 32 channels 97.656 kHz wide, and a central frequency of 1413.8960 MHz corresponding, respectively,

*Kitt Peak National Observatory (KPNO) is a facility of the National Optical Astronomy Observatories (NOAO), operated by the Association of Universities for Research in Astronomy (AURA), Inc., under contract with the National Science Foundation (NSF).

†The Very Large Array is a facility of the National Radio Astronomy Observatory operated by the Associated Universities, Inc., under contract with the National Science Foundation. The VLA is described by Thompson *et al.* (1980).

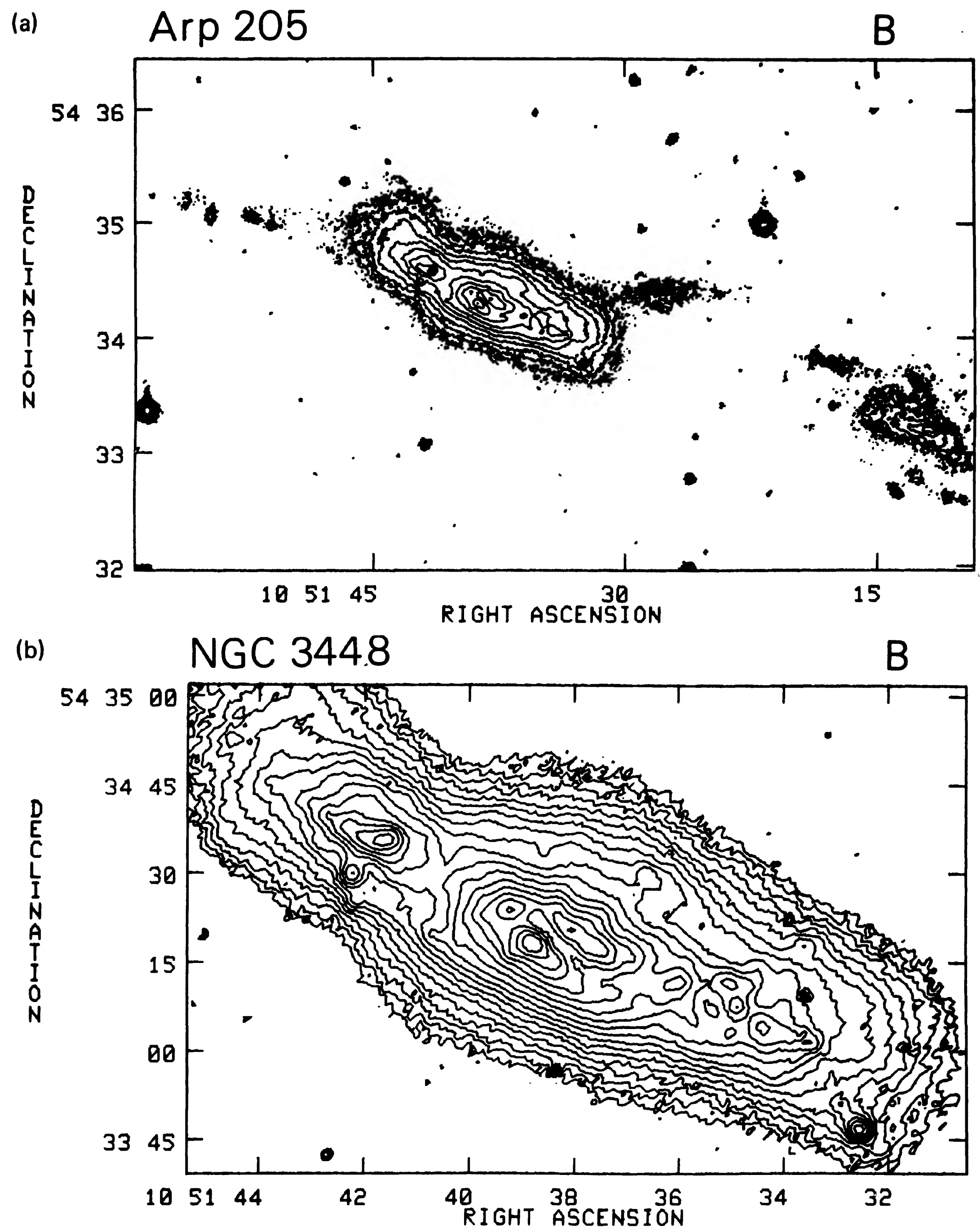


FIG. 1. (a) Calibrated blue picture of Arp 205. The contour levels are from 25 to 19.0 in steps of 0.5 mag arcsec$^{-2}$. Part of UGC 6016 appears in the southwest. (b) Inner area of NGC 3448 in blue light. The contour levels are from 19.5 to 24 mag arcsec$^{-2}$ in steps of 0.25.

TABLE I. Properties of the CCD images.

| Filter | Seeing (″) | Image limit (mag arcsec$^{-2}$) | Center Coordinates h | m | s | ° | ′ | ″ | Exposure length (min) | Date |
|---|---|---|---|---|---|---|---|---|---|---|
| *B* | 2.7 | 24.7 | 10 | 51 | 34.26 | 54 | 34 | 12.0 | 30 | Jan. 21 |
| *B* | 3.2 | 24.4 | 10 | 51 | 36.83 | 54 | 34 | 31.5 | 45 | Jan. 23 |
| *V* | 3.0 | 22.0 | 10 | 51 | 36.85 | 54 | 34 | 30.9 | 30 | Jan. 23 |
| *R* | 2.7 | — | 10 | 51 | 36.64 | 54 | 34 | 30.0 | 15 | Jan. 23 |

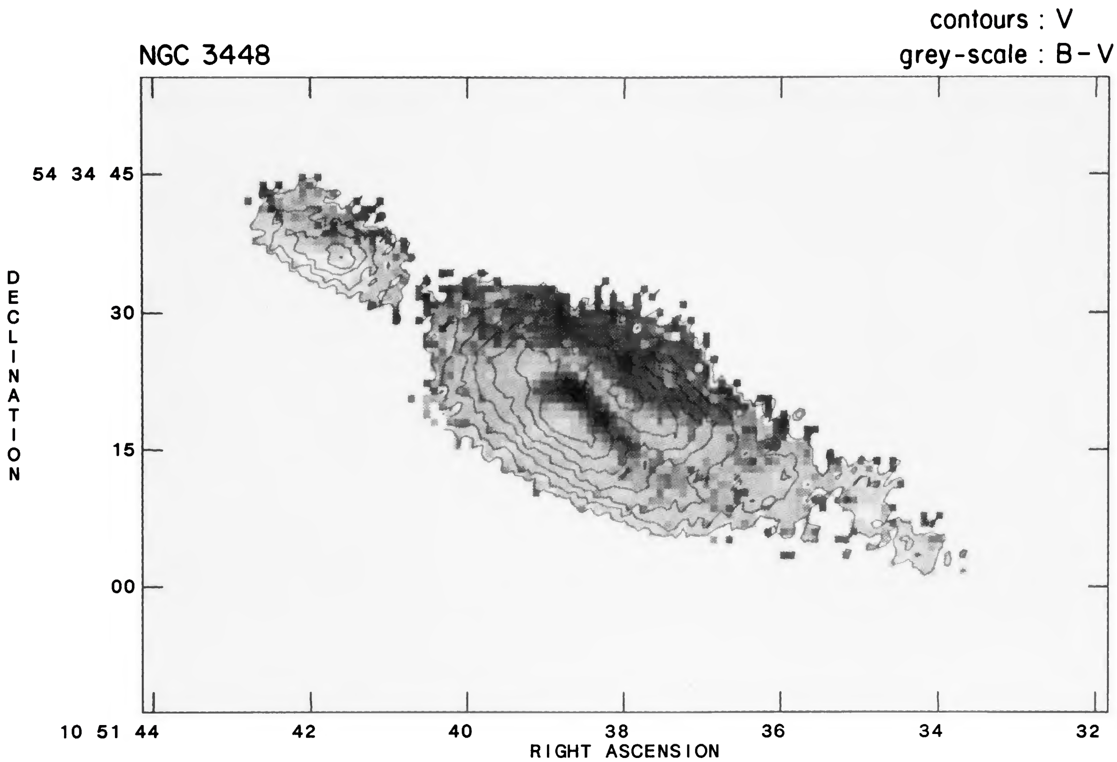


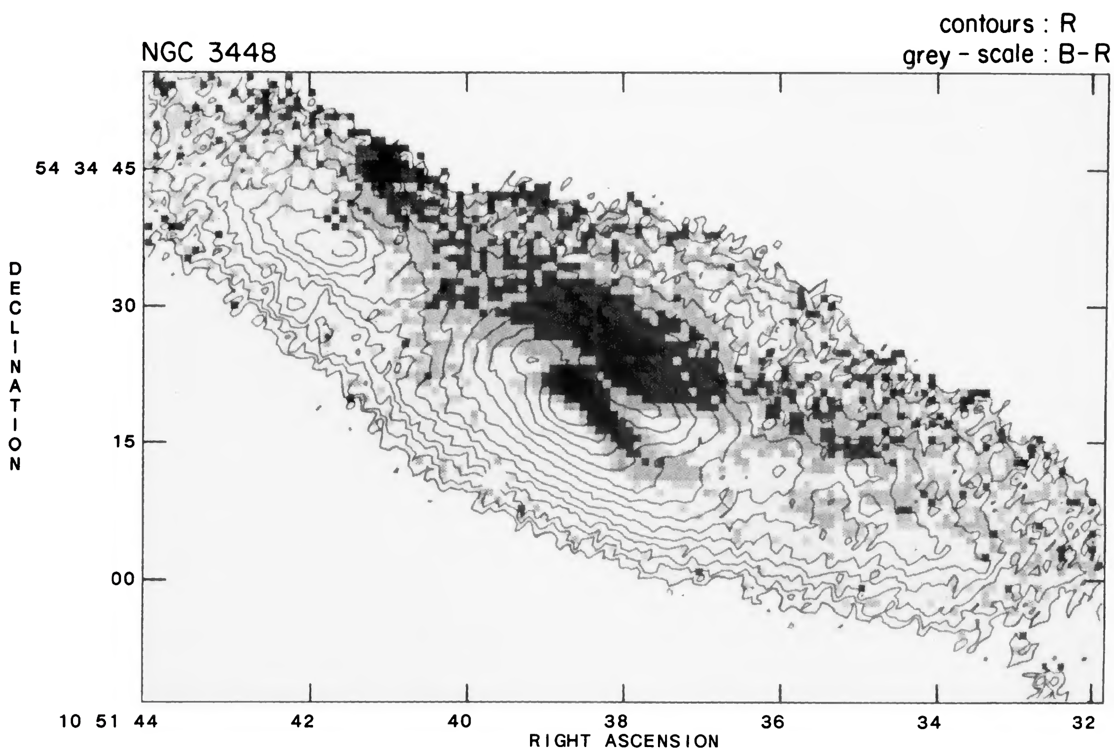


FIG. 2. (a) Contours from the *V* image of NGC 3448 on grey levels showing the *B–V* color index. The contours are from 21 to 19.5 mag arcsec$^{-2}$ in steps of 0.25. The clearest shades of greys correspond to values around 0.2 and the darkest 1.3 in *B–V*. (b) Superposition of contours from the *R* image of NGC 3448 on grey levels showing the noncalibrated *B–R* color index. The contours are spaced by 0.25 mag arcsec$^{-2}$. The clearest shades of grey correspond to the bluest part of the galaxy.

to a velocity width of 20.673 km $s^{-1}$ and a central velocity of 1370 km $s^{-1}$. As usual, channel 0 contained 75% of the band for calibration. The total observed bandwidth of 620.2 km $s^{-1}$ is wide enough to cover the velocity range of both NGC 3448 and UGC 6016 and leave some channels free of spectral-line signal on the red and blue sides of the velocity distribution for the subtraction of the continuum. At the time of the observations, only 21 antennas could be used with 32 channels. The innermost available antennas on each arm were selected.

The phase calibrator was 1031 + 567; 3C 286 was used for both flux and bandpass calibrations. The details of the observations appear in Table II. Autocorrelation normalization was on-line during the observations. The integration time of 60 s is well below the interval recommended by Rots (1982) to avoid "time smearing." Nearly 8 hr of data were collected.

Our calibration included system temperature corrections, channel 0 complex gain calculation, and bandpass calibration with three-channel Hanning smoothing across the band. Finally, the calibrated 32-channel data were recorded on magnetic tapes and transported to Toronto for further processing with the AIPS station.

Maps were generated for each of the 31 spectral channels. Uniform weighting of the data was chosen in order to obtain a better beam shape. After inspection, four channel maps located on the blue side and four on the red side of the velocity field were found to be without line emission. They were averaged together to produce the continuum map which was then subtracted from the other channel maps to form the continuum-free line maps. Because of the very low sidelobe levels ($\sim 1.2\%$) produced by the full-track synthesis no ring lobes were visible above the noise and therefore no "cleaning" of the maps was required.

The line maps are displayed in Fig. 3. To ease the interpretation and further processing the line maps were assembled along a third axis to form the "H I data cube," a three-dimensional matrix of intensity values arranged along one velocity and two spatial dimensions.

The rms noise level is around 1.6 mJy $\text{beam}^{-1}$, in agreement with the predicted noise, estimated from the number of visibility points (Table II). The continuum map has a lower noise, due to its equivalent bandwidth of 0.781 MHz, and was cleaned. The fitted beam is 20.″08 × 17.″08 (1.04 × 0.89 kpc at 10.7 Mpc) oriented at P.A. = − 70.°82; this defines the resolution of these observations. The largest visible structure (limited by the shortest baselines) is about 4′ (12.5 kpc). Arp 205 is small with respect to the primary beam of the VLA antennas at the $L$ band; thus the maps did not need correction for the primary beam attenuation. The velocity resolution of the observation is 24.8 km $s^{-1}$, or 1.2 times the channel separation, since the spectral-line system was operated in the standard mode (Rots 1982).

A map of the total H I distribution was generated using A. H. Rots' MOMNT algorithm described by van Gorkom (1982). This program selects the pixels for the computation (in this case a summation, and can produce average velocity and velocity-dispersion maps) if they are higher than a preselected threshold value when averaged spatially with a Gaussian function, and in velocity with a Hanning function. We used a threshold of 1.4 mJy $\text{beam}^{-1}$, a Gaussian kernel 8 pixels wide, and velocity smoothing over three channels to produce the total H I map. This appears on Fig. 4 together with an optical $B$ image of Arp 205 degraded to the same resolution.

TABLE II. Details of the 21 cm line observations.

| | |
|---|---|
| 3C 286 | |
| flux[a] | 14.764 Jy |
| # of scans | 6 |
| # of visibilities | 3690 |
| length of scans | 3 min |
| 1031 + 567 | |
| flux[b] | 1.841 Jy |
| # of scans | 16 |
| # of visibilities | 8278 |
| length of the scans | 3 min |
| Arp 205 | |
| # of scans | 14 |
| # of visibilities | 70153 |
| length of the scans | 25 min |
| Expected rms noise from the maps | 1.8 mJy $\text{beam}^{-1}$ |

[a] From Baars *et al.* (1977) scale.
[b] Value derived in the calibration.

## III. RESULTS AND DISCUSSION

### *a) Optical Data*

#### *1) NGC 3448*

The light from NGC 3448 is dominated by a luminous "bulge-like body," divided in two elongated regions by a dust lane oriented at a 20° angle from the rest of the galaxy. An unresolved knot stands out in the bulge region almost at the end of the dust lane at R. A. (1950.0) = $10^h 51^m 39.^s21$ and Dec. (1950.0) = 54° 34′ 23.″9. It is called "knot f" by Bertola *et al.* (1984), who suggested that it might be the nucleus of the galaxy. In the southwest side of the central body is a cluster of knots, visible especially in the $B$ pictures. Some of these coincide with positions of H$\alpha$ emission reported by Hodge (1966). Another remarkable feature of this galaxy is the bright patch of light at the NE (peak at R. A. (1950.0) = $10^h 51^m 41.^s6$, Dec. (1950.0) = 54°34′36″).

The tidal appendages visible in Arp's (1966) photograph appear only in the deeper blue CCD images. The $B$ image of 21 January 1983 was smoothed to produce a map with a lower resolution matching the H I observations (Fig. 4). After doing this, the visibility of the tail and bridge of NGC 3448 is improved. The fattening of the last isophotes of UGC 6016 suggests diffuse emission in between its arms. Note also the presence of low-brightness material north of UGC 6016.

The most dramatic feature of the $B - V$ map [Fig. 2(a)] is the systematic north-south color gradient. Using the central dust lane as a boundary, $\langle B - V \rangle = 0.87$ and $\langle B - V \rangle = 0.58$ are derived for the north and the south regions of the galaxy, respectively. The color gradient could be caused by interstellar-dust reddening, or different stellar populations. We suggest dust as the most probable origin for two reasons: (i) Such extended distributions of dust are observed in other amorphous galaxies; (ii) the obscuration occurs in the upper part of the galaxy *which is aligned with the bridge and the tail.* This suggests that some tidal material might lie in front of the galaxy. The color gradient continues across the NE bright patch. Unfortunately, the higher noise level in the $V$ map prevented us from mapping the $B - V$ in the area between the bulge and the NE bright patch. The central dust lane is redder than the northern part of the galaxy with a $\langle B - V \rangle = 0.95$; the material separating knot f from the rest of the bulge is not as red as the dust lane. This suggests that knot f is a separate feature and not just "cut

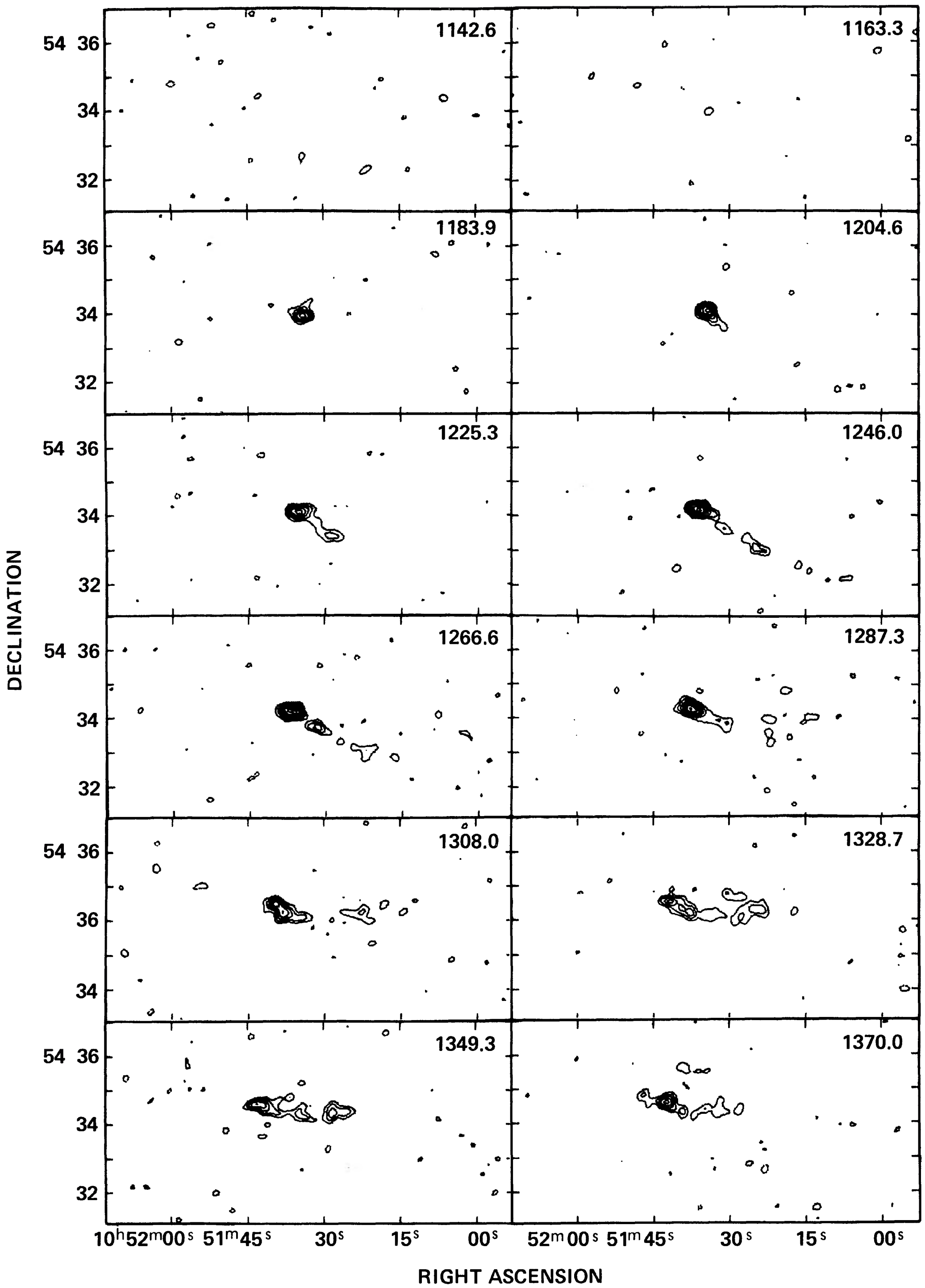


FIG. 3. H I line maps of Arp 205. The levels are − 4.5, 4.5, 7.0, 9.5, 12.0, 14.5, 17.0, and 19.5 mJy beam$^{-1}$. The channel velocity is written in the upper right-hand corner in km s$^{-1}$. The last image is the continuum emission. The beam is 20".08 × 17".08 oriented at P.A. = − 70°.82.

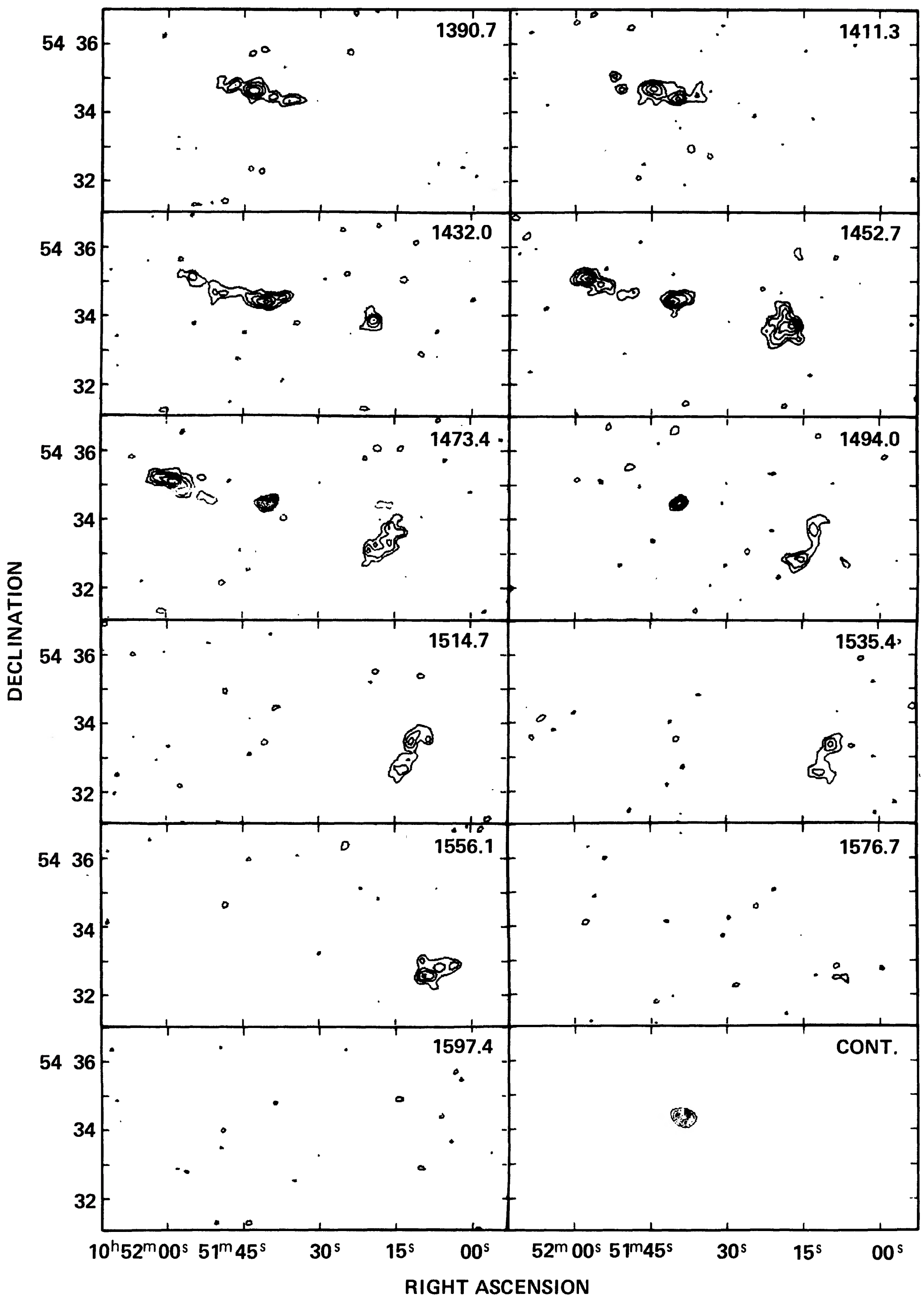


FIG. 3. (continued)

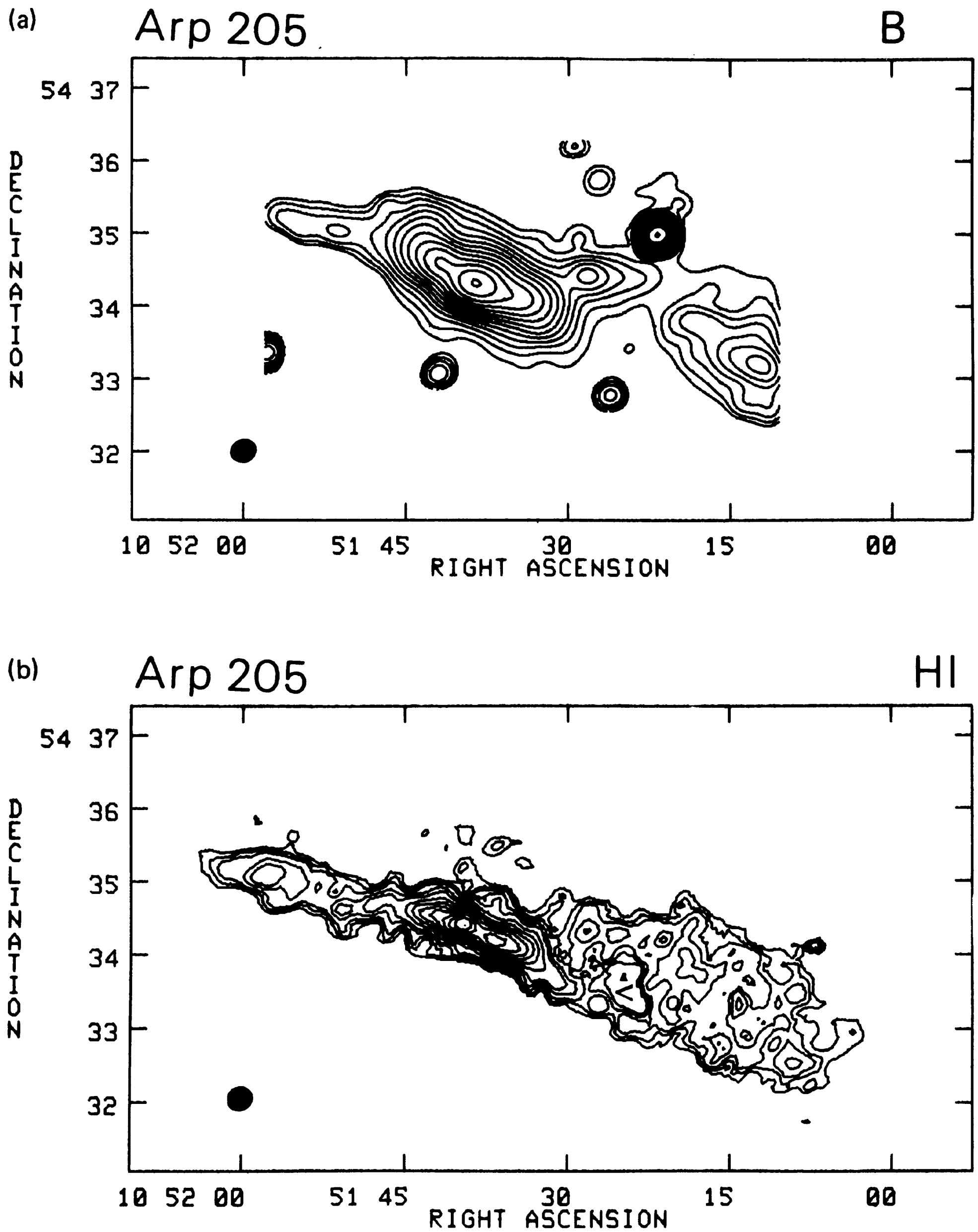


FIG. 4. (a) Optical blue image of Arp 205 smoothed to the same resolution as the beam of the H I observations: 20″.08 × 17″.08 P.A. = − 70°.82. The beam is indicated in the lower left. The contour levels are from 21.0 to 27.0 in steps of 0.5 mag arcsec$^{-2}$. (b) Total H I map; the contours are 5%, 7.5%, 10%, 15%, 20%, 30%, 40%, 50%, 60%, 70%, 80%, 90%, and 100% of 3.27 Jy beam$^{-1}$ km s$^{-1}$, 1.05 $\times 10^{22}$ hydrogen atoms cm$^{-2}$, or 84.4 $M_{\odot}$ pc$^{-2}$ of neutral hydrogen.

away" from the bulge by the dust lane. At its peak this knot has a $B - V = 0.42$, whereas the southern part of the NE patch has a $\langle B - V \rangle = 0.40$. The color of the southern part of NGC 3448 suggests vigorous star formation. The mean color of spiral arms of late-type galaxies obtained by Schweitzer (1976) is $\langle B - V \rangle = 0.59$.

Due to the better signal-to-noise ratio of the $R$ map, a larger portion of the galaxy is visible with the uncalibrated $B - R$ maps. This map also shows the reddening of the dust lane, the blue knot f, and the color gradient across the galaxy. North of the bulge, the galaxy reverts to bluer colors; this further supports our hypothesis that an elongated cloud lies in front of the galaxy. The area between the bulge and the NE patch is reddened, suggesting that the bright northeastern patch belongs to the galaxy and is not a foreground dwarf galaxy. The southern part of the NE patch appears again on the uncalibrated $B - R$ map as the bluest portion of the galaxy. The cluster of knots is visible in the uncalibrated $B - R$. These appear to have intrinsically blue colors.

*2) The companion galaxy UGC 6016*

A large portion of UGC 6016 was included in the $B$ image of the 21 January 1983 frame (see Figs. 1 and 8, expanded scale). The galaxy's light is dominated by an asymmetric central bar, which is also visible in the lowest levels of the $R$ picture. The brightest point of the galaxy lies in the bar at R. A. (1950.0) = $10^h 51^m 12^s$ and Dec. (1950.0) = 54° 33′ 13″. In the red picture, the maximum is found within one pixel of the same position. We suggest that it is the optical nucleus. The spiral arms are very patchy, and a chain of H II regions can be identified in the northeast. In Fig. 1 the spiral arms seem to originate from the middle of the bar, contrary to what is usually observed in smoothed images, suggesting an underlying smooth luminous disk. The surface-integrated blue magnitude of the portion of UGC 6016 present on the $B$ image is 15.1 $m_B$ (CCD instrumental $B$ magnitude). At the de Vaucouleurs (1975) distance of 10.7 Mpc, the absolute magnitude will be $M < -15$, which compares with Tammann's (1980) luminosity limit($M > -16\ m$) for dwarf galaxies. UGC 6016 appears to be a genuine DSp according to van den Bergh's definition (van den Bergh 1959).

### *b) Distribution of H I in the Arp 205 System*

NGC 3448, the central structure on the velocity maps of Fig. 3, is found in velocity ranges from 1163.3 up to 1514.7 km $s^{-1}$. Its companion, UGC 6016, is visible from 1411.3 up to 1576.7 km $s^{-1}$ south-preceding. The anomalous velocity feature—the hump in the velocity curve of Bertola *et al.* (1984)—lies near R. A. (1950.0) = $10^h 51^m 40^s$ and Dec. = 54° 34′ 28″ and in the velocity range from 1411.0 up to 1514.7 km $s^{-1}$.

There is no continuous stream of gas from NGC 3448 to UGC 6016. This contrasts with the flows observed between other galaxies (e.g., M81 and NGC 3077; van der Hulst 1979). Gas connected to NGC 3448 coincides in position with UGC 6016, but is actually rushing away from the dwarf with a line-of-sight component of 200 km $s^{-1}$.

The flux at different velocities was calculated by integrating a set of spectral maps smoothed to a resolution of 50″ in order not to miss any diffuse extended structure. The H I profile of Arp 205, broken into the contributions of NGC 3448 and UGC 6016, is displayed in Fig. 5. Our H I profiles reproduce well the shape of the integrated profiles published by Peterson and Shostak (1974) and Huchtmeier and Bohnenstengel (1975). The peak around 1460 km $s^{-1}$ and the 60 km $s^{-1}$ "skirt" on the right are explained by contamination from UGC 6016. The individual profiles of UGC 6016 and NGC 3448 show more normality than the overall shape of the Arp 205 profile but clearly differ from the classical double-horned profiles.

Listed in Table III are the total H I mass* derived from our observations along with estimates from previous authors to a common distance of 10.7 Mpc. Our result for the H I mass in the pair agrees well with the single-dish measurements, but is lower than the values of Bottinelli *et al.* (1978) made with the Nançay telescope and Reakes (1979) with the Cambridge Half-Mile telescope. Some flux from large-scale structure might have been missed due to the insensitivity of the array to structures larger than 4′ and our use of a cutoff technique. On the POSS prints no galaxies appear north or south of Arp 205 which could explain the higher H I flux from Nançay. The higher H I mass for UGC 6016 from Reakes (1979) cannot be explained except by invoking noise-related errors in his maps. We discuss NGC-3448 and UGC 6016 in turn below.

#### *1) NGC 3448*

The signal from UGC 6016 in the H I data cube was blanked out to create a subcube with emission originating only from NGC 3448. The total H I map was computed and is displayed in Fig. 6. The body of NGC 3448 is barely resolved in the $z$ direction. The transverse width of the body of NGC 3448 in H I is slightly smaller than in the optical at full resolution (Fig. 1), and even smaller compared to the optical image at matched resolution (Fig. 1). Thus despite the interaction a large part of the neutral hydrogen *lies in the plane of the galaxy.*

The most striking difference between the optical and radio maps is probably the extent of the tidal H I west of the main body of the galaxy. High-resolution and smoothed optical images of Arp 205 were searched at the same location for corresponding optical features. None were found at an upper limit of 27 mag arcsec$^{-2}$. The optical west bridge of NGC 3448, although shorter, coincides well with a density enhancement in the H I image. Also, the east tail is also more extended in H I than in the optical, even for smoothed optical images. In H I, it lies slightly to the south of the optical tail. The tail is visible in the velocity range from 1390.0 to 1411.3 km $s^{-1}$. At the lower velocities it coincides well with the optical emission, but the centroid of the H I emission moves south at higher velocities.

A velocity-dispersion map was also produced. In the body

*The total H I mass is calculated from the standard formula: $M_{\rm H\,I} = 2.356 \times 10^5 D^2 \int_v S_v\ dv$. $M_{\rm H\,I}$ is in $M_\odot$, $D$ the distance in megaparsecs, $S$ the flux in Jansky at velocity $v$ (km $s^{-1}$). Wright (1974) gives a derivation. The use of this formula assumes that the gas is optically thin and that there is no interaction between continuum and line emission.

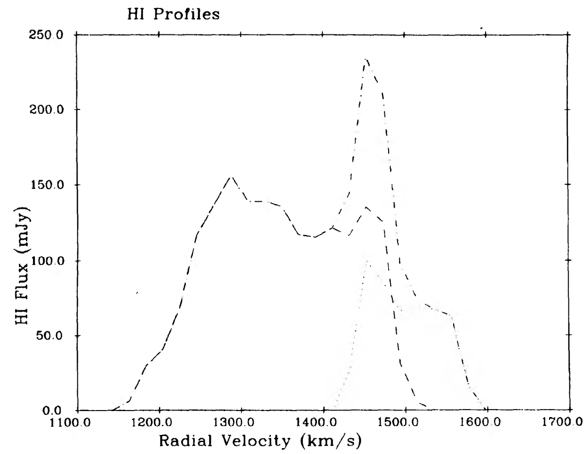


FIG. 5. H I profiles for the Arp 205 system; the dash, dotted, and dot-dash lines are for the emission of NGC 3448, UGC 6016, and Arp 205, respectively.

TABLE III. H I mass of Arp 205.[a]

| Arp 205 | NGC 3448 | UGC 6016 | Telescope and authors |
|---|---|---|---|
| 1.53 | 1.20 | 0.33 | The Very Large Array<br>This study |
| 1.5[b] | — | — | Green Bank 91 and 43 m<br>Davis and Seaquist 1983 |
| 2.2 | 1.15 | 0.68 | Cambridge Half-Mile<br>Reakes 1979 |
| 2.18 | 1.82 | 0.36 | Nançay<br>Bottinelli *et al.* 1978 |
| 1.6 | — | — | Effelsberg 100 m<br>Huchtmeier, Bohnenstengel 1975 |
| 1.7 | — | — | Green Bank 91 m<br>Peterson and Shostak 1974 |
| 1.7 | — | — | Bank Mark I and II<br>Lewis and Davis 1973 |

[a] All the H I mass estimates are in $GM_\odot$ for a common distance of 10.7 Mpc.
[b] Mean values from different telescopes, corrected for beam size.

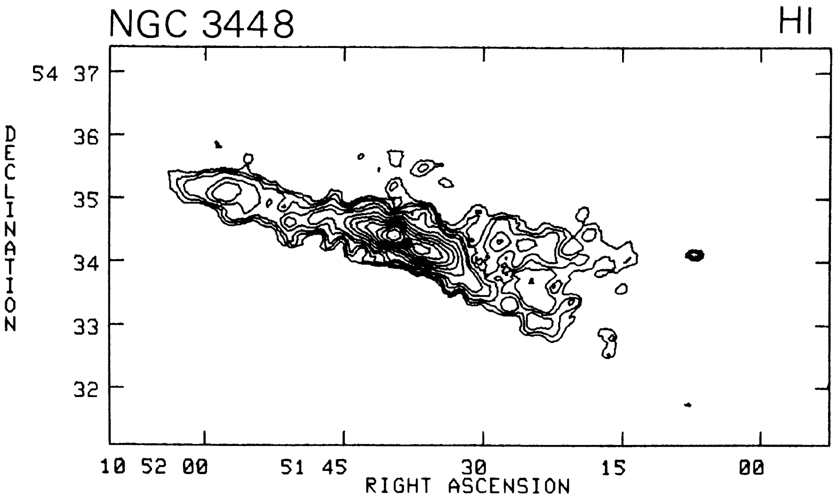


FIG. 6. Total H I from NGC 3448 only, the contours are as in Fig. 5. The dot indicates the position of the central point source, R. A. (1950.0) = $10^h\,51^m\,38\overset{s}{.}62(0\overset{s}{.}17)$, Dec. (1950.0) = $54°34'20\overset{''}{.}0(1\overset{''}{.}4)$.

of the galaxy, because of the double velocity profiles the velocity dispersion is meaningless. The velocity dispersion in the tail is less than 25 km $s^{-1}$ and is also low (less than 15 km $s^{-1}$) in the rather complex spray-like bridge. The H I mass of the hump cloud was redetermined. The new value of $M_{\rm H\,I} = 8.4\times 10^7\,M_\odot$ supercedes the slightly lower value of Bertola *et al.* (1984).

The first velocity curves at P. A. = 60° (Bertola *et al.* 1984) are well aligned with the brightest optical part of the galaxy, but the large-scale features of NGC 3448—the tidal extensions—define an axis of symmetry at P. A. = 74°. The H I cube was interpolated to produce a new cube whose spatial dimensions would be parallel and perpendicular to this large-scale symmetry axis. Afterward, we generated a family of velocity-position-intensity plots along the long axis at different positions on the short axis by isolating different planes in the new cube. These plots (Fig. 7) are offset by 4″ (the pixel size) with respect to R. A. (1950.0) = $10^h\,51^m\,32^s$ and Dec. (1950.0) = 54°34′20″. The most interesting one is for the position at + 12″, which shows a new well-developed double velocity profile. This velocity profile appears connected to the "tidal bridge" and also the hump cloud. Furthermore, it coincides spatially with the very reddened region in the northern portion of the bulge. Similar families of position-velocity intensity plots (not shown) were created for P. A. = 60° and 90°. On the latter, it is clear that the *double velocity profile is linked to the H I counterpart of the optical bridge and continues across the body of the galaxy.* The $x$ axis of the velocity-position plots at P. A. = 74° is parallel to the tail and thus describes the rotation of the tail. The plots labeled − 20″ to + 12″ contain most of the emission from the tail, and the velocity curve flattens to a constant velocity ($\sim 1475$ km $s^{-1}$). Thus the material in the tail does not partake in the solid-body rotation of the inner part of NGC 3448.

*The mass of NGC 3448*: The determination of the dynamical mass of NGC 3448 is difficult due to the complex H I distribution and velocity structure. We will assume that the inner part of the galaxy which shows solid-body rotation is unaffected by the interaction and estimate the mass in the inner part of the galaxy. We will refer directly to the terminal velocity to estimate the mass as is done for the Milky Way and edge-on galaxies (cf. Sancisi and Allen 1979 or Weliachew *et al.* 1978), and correct for the 74° inclination of NGC 3448. A satisfying rotation curve can be drawn (Noreau 1985) over the velocity-position plot at 60°. The apparent terminal velocity is $\sim 120$ km $s^{-1}$ at a distance of $\sim 55''$ or $\sim 2.9$ kpc from the galaxy center. The central velocity is 1300 km $s^{-1}$. This is lower than the median value from the velocity profile (Fig. 5) of 1340 km $s^{-1}$.

Lequeux (1983) suggests measuring the mass inside a radius using: $M(R) = (0.6 \text{ to } 1.0)(RV^2(R)/G)$. The first expression on the right-hand side of the equation will be called the Lequeux fudge factor. The minimum value corresponds to the limit case for a galaxy made of a disk plus a bulge from Nordsieck's (1973) analysis, while the maximum value is for spherically distributed matter (massive dark halo). Lequeux (1983) argues that the accuracy of the mass *inside a given radius* will be limited more by errors in the radial velocity, inclination, distance, and noncircular motions than by characteristics of the mass model.

After correction for the inclination, we derive a final mass of 8.4 $GM_\odot$ using a Lequeux fudge factor of 0.8 for the inner part of the galaxy. The H I contained in the central portion of the galaxy accounts for about 30% of the total H I mass detected, which is 4.3% of the total mass of the inner part of a galaxy. The rest of the H I is found mainly in the tidal structure; of which almost 10% makes up the hump cloud. In Bertola *et al.* (1984), a mass of 5.3 $GM_\odot$ was derived using a spheroid with a flattening of 0.2.

An estimate of the total mass of NGC 3448 can be obtained using Faber and Gallagher (1979) galaxy mass-to-light ratios. NGC 3448 can probably be considered as a late-type galaxy because of its blue colors (Larson and Tinsley 1978) and the absence of a dominating bulge. The mass-to-light ratios of Faber and Gallagher (1979) need to be corrected to the short distance scale and for the adopted Lequeux fudge factor of 0.8. The total mass estimates we find for Scd–Sd and Sdm–Irr galaxies are, respectively, 26 and 11 $GM_\odot$ (using the RC2 corrected blue magnitude of $B_T^0 = 11.59$). These estimates are consistent with the dynamical mass for the inner part of NGC 3448. For both galaxy types we can derive H I mass to total mass ratios $M_{\rm H\,I}/M_{\rm T} = 4.7\%$ and 10.8%, respectively. The distance-independent H I mass-to-luminosity ratio for NGC 3448, $M_{\rm H\,I}/L_{\rm pg} = 0.29\,M_\odot/L_{\odot\rm pg}$. According to Roberts (1972),

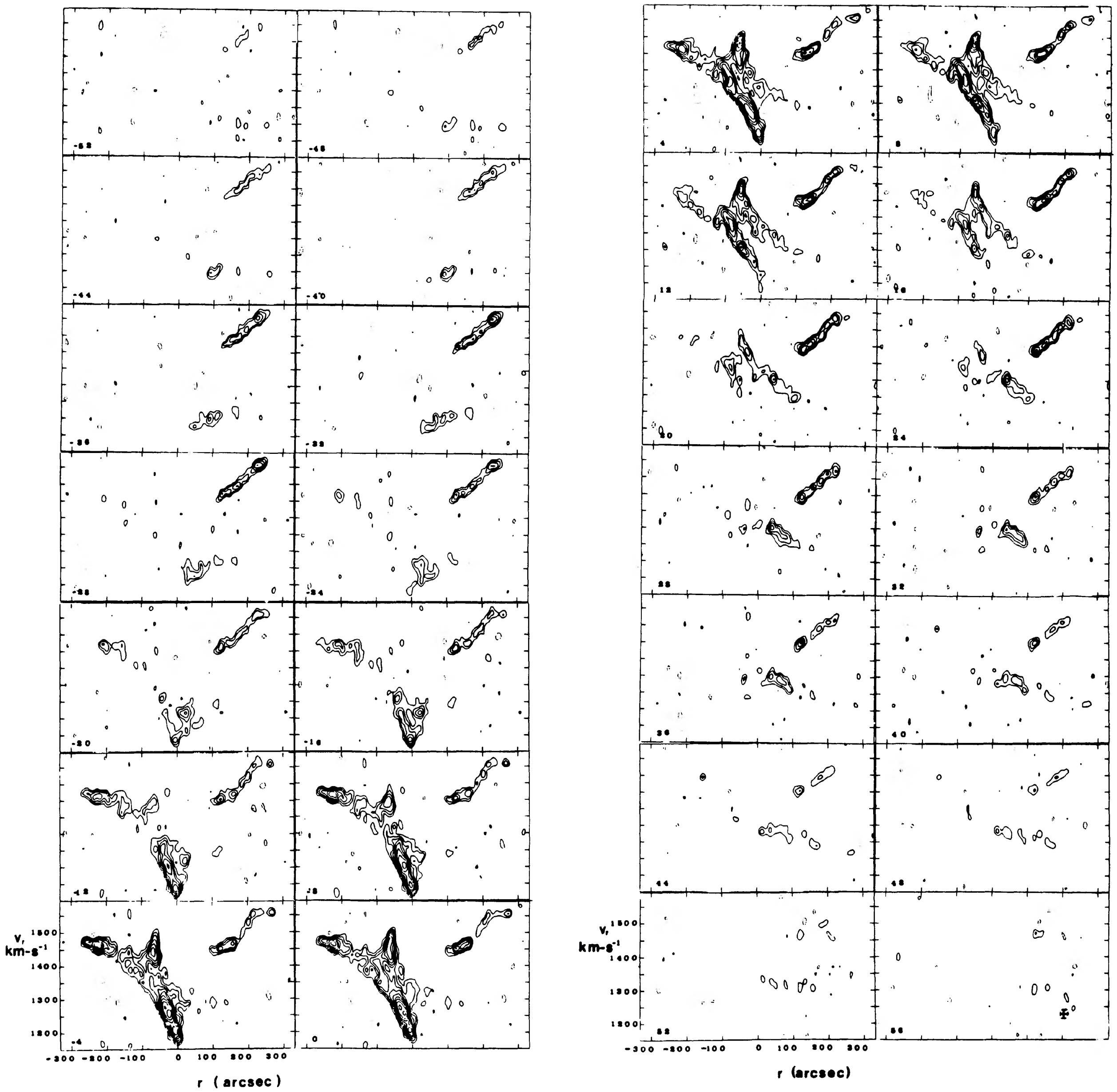


FIG. 7. Position-velocity plots of NGC 3448 oriented along P.A. = 74° at different positions along the minor axis. The contour levels are − 4, 4, 6, 8, 10, 12, 14, 16, 18, and 20 mJy beam$^{-1}$. The double velocity feature is clearly visible in the frames from positions 4 to 16.

it would be consistent with Sbc galaxies. However, it should be recalled that we are dealing with an unusual object, and that the integrated properties of normal galaxies might not necessarily apply.

*2) UGC 6016*

A subcube 352″ in right ascension, 320″ in declination, and 186 km s$^{-1}$ in velocity was "cut out" from the H I data cube to isolate UGC 6016. We generated maps of the total H I column density, mean velocity, and velocity dispersion of UGC 6016 using the same parameters as for Fig. 4(b). The first two are displayed in Fig. 8 along with optical images both at high resolution and smoothed to the H I distribution. The extent of the optical emission in the smoothed map is not significantly smaller than the neutral-hydrogen distribution. There is a coincidence between the chain of H II regions in the northwest spiral arm with a density enhancement in the total H I map. A less important enhancement is visible on the other side of the galaxy and seems to correspond to the SW spiral arm (not visible in our images). The bar in UGC 6016 does not coincide with any particular feature in the total H I map. There is less H I in the center, but UGC 6016 does not have a hole as is found in the large spiral galaxies. It is thus similar to the dwarfs observed by Tully *et*

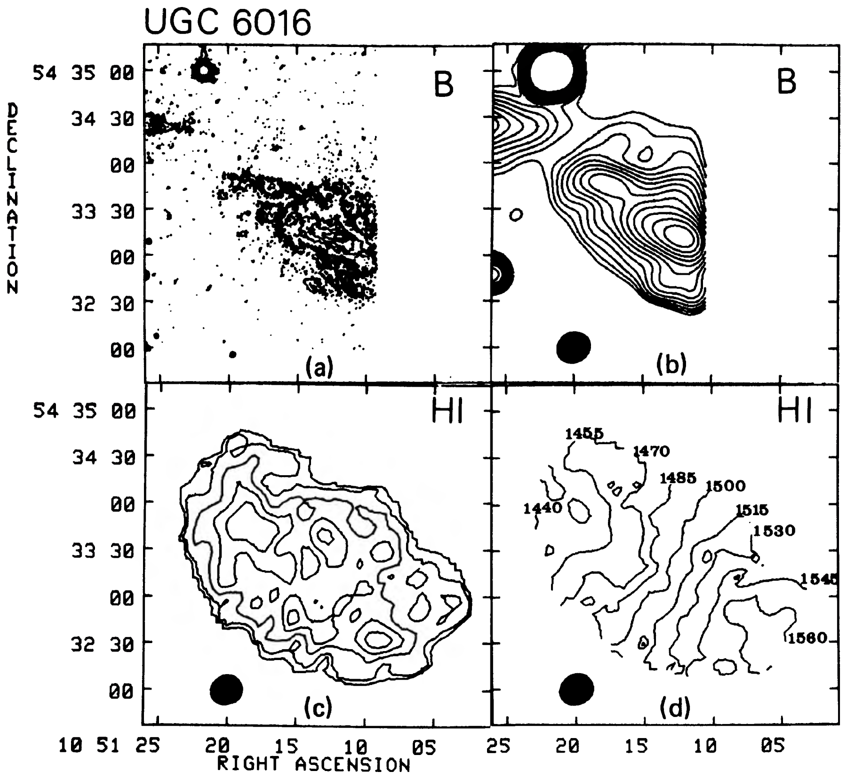


FIG. 8. (a) UGC 6016 seen partially in blue light; the contour levels are from 22 to 25 mag arcsec$^{-2}$ by step of 0.5. The resolution is about 3″. (b) UGC 6016 smoothed to the resolution of the H I observations; the beam appears in the lower left-hand corner. The magnitude contour levels range from 17 to 24 mag arcsec$^{-2}$ in steps of 0.25. (c) Total H I in UGC 6016; the contours are 10%, 20%, 40%, 60%, and 100% of the maximum 0.580 Jy beam$^{-1}$ km s$^{-1}$ or $1.81 \times 10^{21}$ hydrogen atoms cm$^{-2}$ or 15.0 $M_\odot$ pc$^{-2}$ of neutral hydrogen. (d) Velocity field of UGC 6016; the contours range from 1440 to 1560 km s$^{-1}$ in steps of 15 km s$^{-1}$.

*al.* (1978). The outer contours of the H I map are slightly elliptical, which allows us to define a major axis oriented at P. A. = 55°. The major and minor axes in the total H I column density map are, respectively, 196″ and 117″ long. The derived inclination (using $\sec(i) = a/b$), is $i = 53\overset{\circ}{.}3$ assuming an axisymmetric H I distribution.

The velocity field is symmetric with respect to the major axis, with a hint of a small s-shaped disturbance. However, features such as the bar or the arms which could cause noncircular motions are barely resolved by the synthesized beam (cf. Fig. 8).

The velocity-dispersion map (not shown) has a mean value of 9.2 km s$^{-1}$. The areas with velocity dispersion higher than 15 km s$^{-1}$ lie in the central region where the H I density is lower. Such values of velocity dispersion are similar to those observed in normal galaxies.

We calculated the rotation curve of UGC 6016 by fitting a Brandt (1960) curve to the average velocity map using a projection method first described by Warner *et al.* (1973). This procedure is well suited to UGC 6016's regular velocity field and favorable inclination. The central position, position angle of the major axis, inclination of the plane, systemic velocity, maximum velocity and radius at which it occurs, and the exponent $n$ was fitted by the model (Table IV). The fitted curve appears in Fig. 9. The center of the velocity field calculated is 11″ east from the optical nucleus but still in the bright bar.

The rotation curve shows a rigid-body portion followed by a flatter segment. The bump found in some large galaxies is absent. The radius inside which the rotation appears to be a purely rigid body as estimated by eye is even smaller: 50″ (2.6 kpc). The rotation curve resembles others found in

TABLE IV. Fitted parameters of UGC 6016.

| | |
|---|---|
| Center position | $10^h51^m13\overset{s}{.}3(\overset{s}{.}2)$,54°33′11″(2″) |
| Major axis P.A. | 59°(1°) |
| Inclination | − 53°(3°) |
| Systemic velocity | 1504(1) km s$^{-1}$ |
| $v_{max}$ | 79(3) km s$^{-1}$ |
| $R_{max}$ | 108″(25),5.6(1.3) kpc |
| $n$ (Brandt exp.) | 1.6(0.6) |

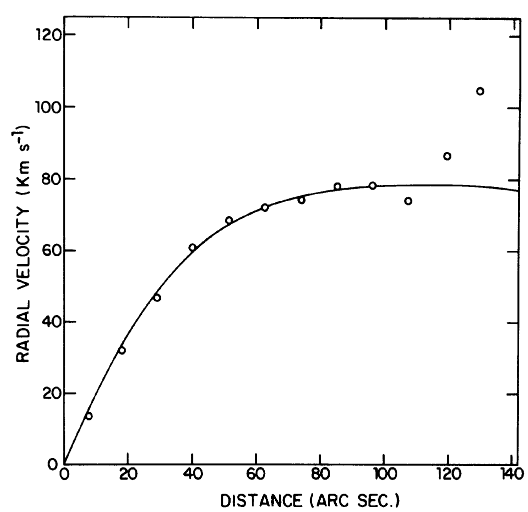


FIG. 9. Velocity curve with a Brandt model. At 10.7 Mpc, 20″ is 1.04 kpc.

dwarf irregular galaxies (Tully *et al.* 1978). We evaluated the mass inside the well-determined portion of the rotation curve, i.e., inside 100″ (5.2 kpc). The velocity from the exponential curve at that point is 80 km s$^{-1}$, which yields a mass of $M_{100''} = 6\ GM_{\odot}$ using a Lequeux fudge factor of 0.8 as for NGC 3448. The total mass estimate using the Brandt (1960) formula is $M_T = 18\ GM_{\odot}$, but the mass estimate inside 100″, $M_{100''} = 6\ GM_{\odot}$, can be derived for the Brandt curve by interpolating the tables of Brandt and Scheer (1965).

The H I mass to dynamical mass ratio for UGC 6016, $M_{\rm H\,I}/M_{100''} = 0.05$, is low for Sp–Irr dwarf galaxies (cf. Tully *et al.* 1978). The mass inside 100″ ranks the galaxy among the more massive dwarf galaxies. The dynamical mass to photographic luminosity ratio (using $B_T^0 = 14.8$), $M_{100''}/L_{\rm pg} = 28\ M_{\odot}/L_{\odot}$* is relatively large when compared to the sample of Tully *et al.* (1978), but is still less than the values of Lake and Schommer (1984). Finally the (distance-independent) ratio of the neutral-hydrogen mass to photographic luminosity $M_{\rm H\,I}/_{\rm pg} = 1.5\ M_{\odot}/L_{\odot}$ is comparable to the values reported by Tully *et al.* (1978). We suggest that the luminosity of UGC 6016 might be too low due to some probable obscuration by tidal material from NGC 3448 (cf. Figs. 4 and 6).

## IV. MODEL OF THE NGC 3448-UGC 6016 INTERACTING GALAXY SYSTEM

To improve our understanding of the geometry of NGC 3448/Arp 205, we generated models of the system with a restricted three-body simulation of the type used by Toomre and Toomre (1972). We note that the restricted three-body model has the limitation that it ignores the self-gravity component of the response of each galaxy to the perturbing field and the back reaction of this response on the galaxy cores. A consequence of this being that the relative radial velocity of the galaxy cores cannot be reproduced. However, according to Combes (1978), this type of simulation is especially good at reproducing the behavior of the gas in interacting galaxies.

### *a) Constraints on the Model*

The relative isolation of Arp 205 eases our modeling task, since the dynamical effects involve only two galaxies. The main observationally determined physical parameters in the model are summarized in Table V. Our model treats UGC 6016 as a point mass.

For significant tidal effects to occur, the mass ratio of the two objects must be relatively close to one, and the eccentricity must be relatively near unity. Our model must produce the following observed features: (i) the absence of a material bridge between the two galaxies, (ii) the pericenter distance should be large enough so that material in the two disks is not slowed down by dynamical friction, and (iii) the model must explain the anomalous disturbed features of NGC 3448, both in space projection and velocity.

We make the reasonable assumption that the mean radial velocity of the global H I profile of Arp 205 is close to the center-of-mass velocity. We can estimate a mass $\sim 20\ GM_{\odot}$ using the radial velocity of all the gas in NGC 3448. This fits inside the range obtained using galaxy mass-to-light ratios. Using a simple-minded two-body approximation, a lower limit on the energy can be derived which corresponds to an

*The absolute $B$ magnitude of the Sun is set to be 5.48, as in Faber and Gallagher (1979).

TABLE V. Physical parameters of the pair.[a]

| | | |
|---|---|---|
| NGC 3448 | | |
| Mass (inner part) | | 8.4 $GM_{\odot}$ |
| Total mass estimate | | 10–40 $GM_{\odot}$ |
| Rigid-body rotation radius | 55″ | 2.9 kpc |
| Length of the inner body | 165″ | 8.6 kpc |
| Total length | 440″ | 22.8 kpc |
| Radial velocity | | 1340 km s$^{-1}$ |
| Radial velocity (inner part) | | 1300 km s$^{-1}$ |
| UGC 6016 | | |
| Mass inside 100″ | | 6 $GM_{\odot}$ |
| Radial velocity | | 1504 km s$^{-1}$ |
| Arp 205 | | |
| Projected optical separation[b] | 245″ | 12.7 kpc |
| Projected dynamical separation[c] | 242″ | 12.5 kpc |
| Radial velocity of the center of mass | | 1374 km s$^{-1}$ |

[a] All quantities are for a distance of 10.7 kpc.
[b] The optical separation is the distance from the nucleus of UGC 6016 to the center of the dust lane in NGC 3448.
[c] The dynamical separation is the distance between the centers of rotation of UGC 6016 and NGC 3448.

eccentricity $e < 1.8$ for the galaxy orbit. An estimate of $R \simeq 13$ kpc is obtained for the value of the pericenter with the same type of approximation.

### *b) The Model*

We used the same geometry as for Toomre and Toomre (1972) (their Fig. 6). The time is set to zero at the pericentric passage. The programs were thoroughly tested, and could reproduce the most convoluted geometries in TT.

Simulating the dynamics of NGC 3448 involved the exploration of a parameter space of 12 dimensions. After many attempts, a model which satisfactorily reproduces most of the large-scale features of NGC 3448 relative to its interaction with UGC 6016 was obtained. It is displayed in Fig. 10, and its evolution is shown in Fig. 11. Table VI lists the parameters of the model. We chose not to model UGC 6016 since it was only mildly, if at all, affected by the interaction. This is easily explained by its observed counterrotation with respect to its passage near NGC 3448 (cf. Toomre and Toomre 1972).

Prior to the interaction, the victim galaxy is a disk 8.0 kpc in radius comprising 500 test particles randomly distributed. The density of points was set to be constant from the center of the galaxy to its edge in order to enhance the visibility of

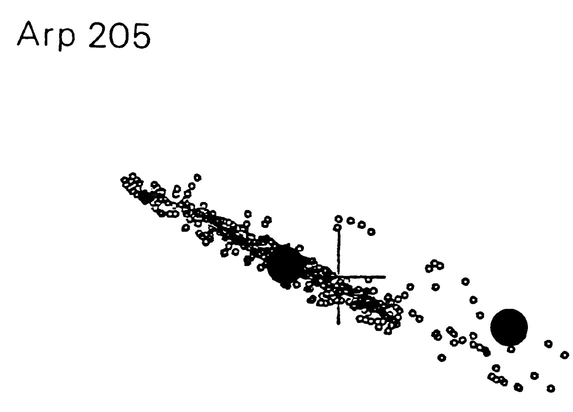


FIG. 10. Model of Arp 205; the galaxy cores are shown by the black dots. The cross lies at the center of mass of the system.

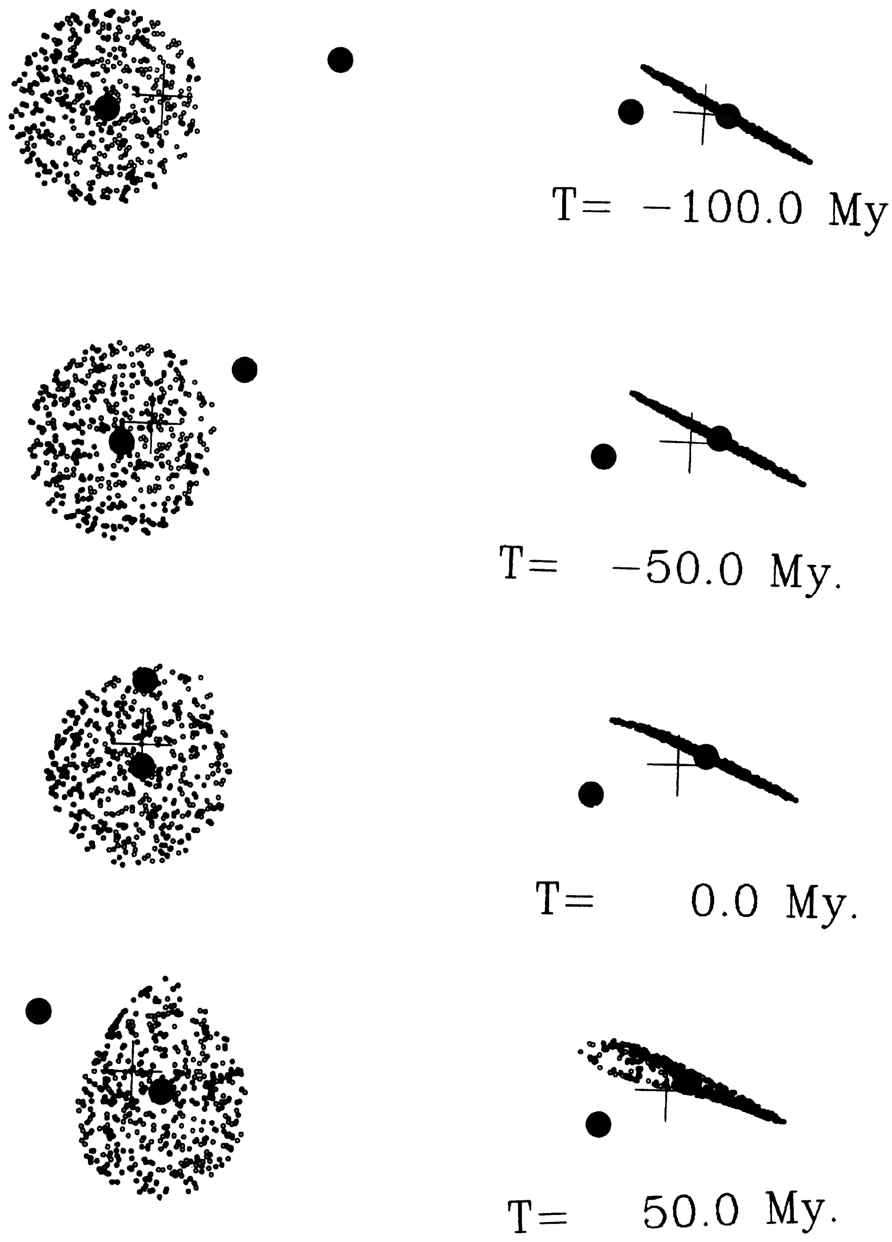


FIG. 11. Time steps in the formation of NGC 3448 as calculated by our most successful model. The view on the left is from directly above the disk of NGC 3448. The view on the right is from where the galaxy is currently observed. Here again the cross indicates the center of mass. The origin of time is the pericentric passage.

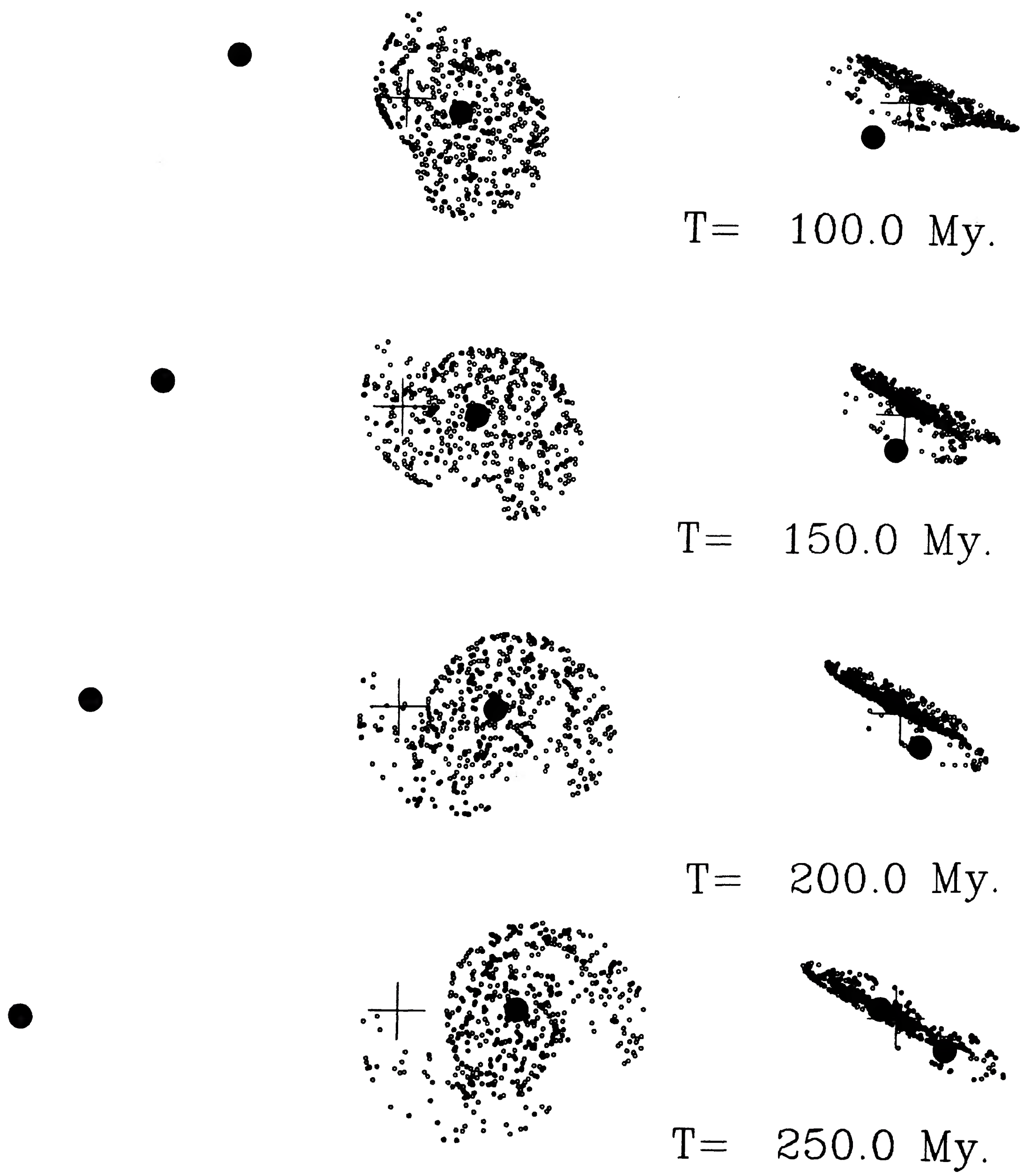


FIG. 11. (continued)

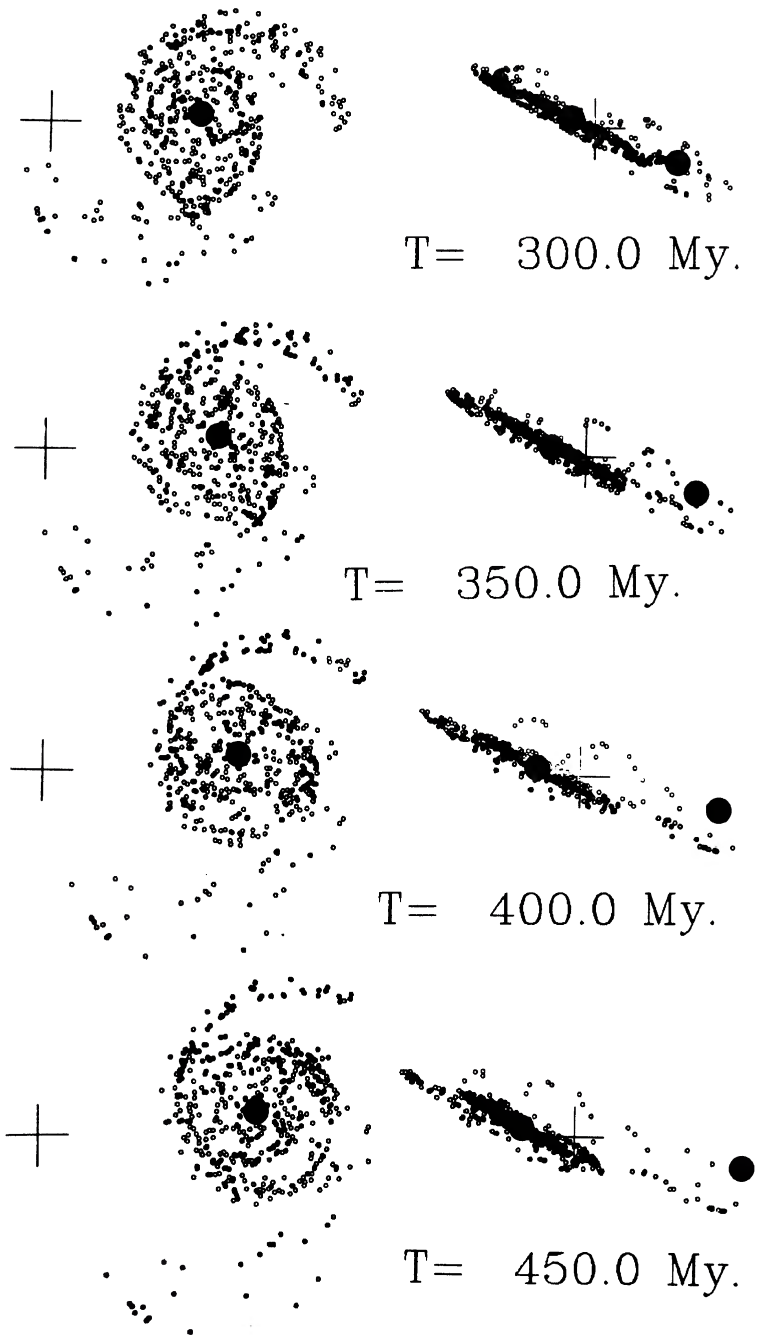


FIG. 11. (continued)

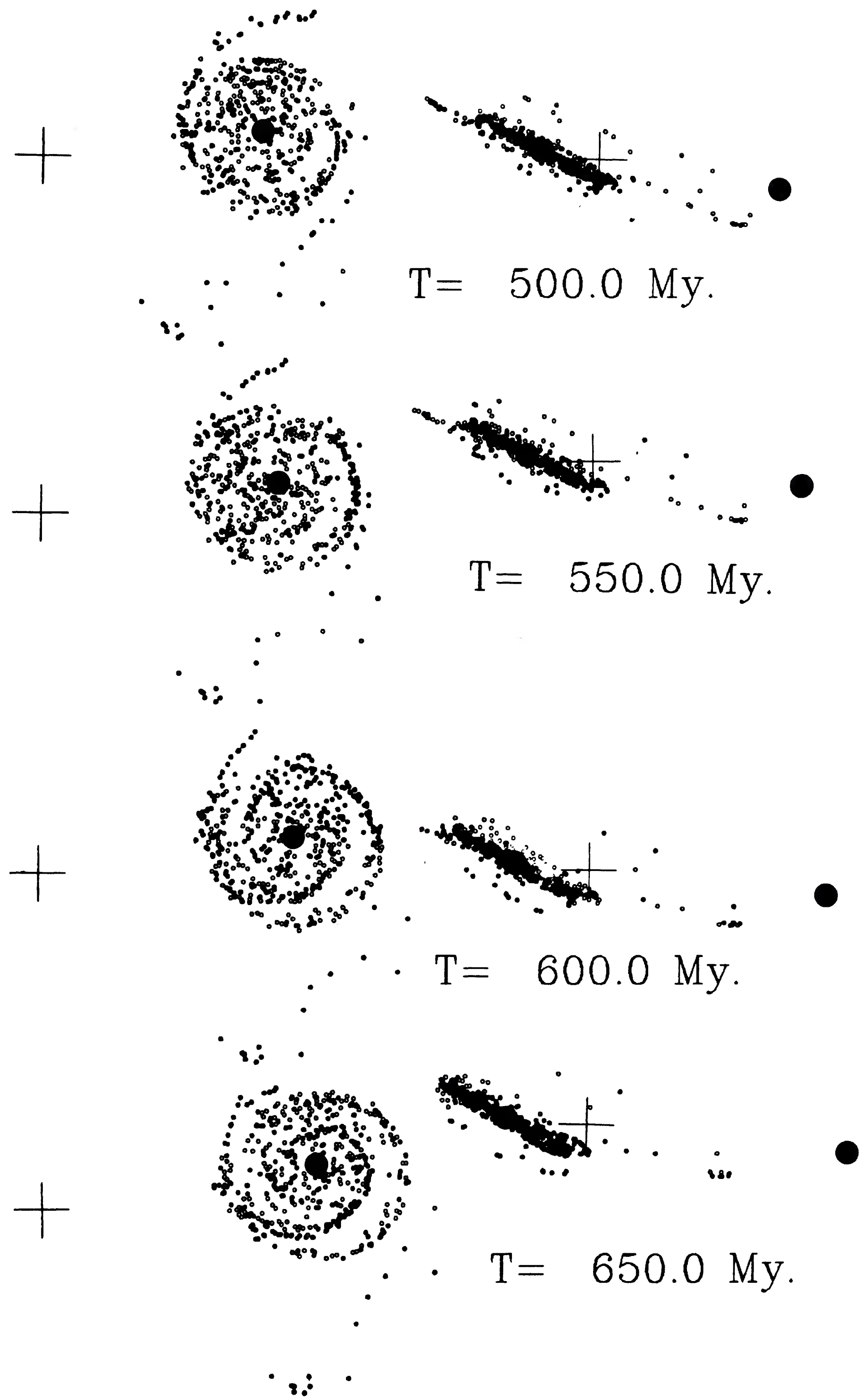


FIG. 11. (continued)

TABLE VI. Parameters of the model.

| | |
|---|---|
| Victim Galaxy | |
| Total mass | 19 $GM_\odot$ |
| Diameter before the collision | 16 kpc |
| Brandt velocity law | |
| $R$ | 2.9 kpc |
| $V$ | 120 km s$^{-1}$ |
| $n$ | 1.84 |
| Perturbing object (UGC 6016) | |
| Total mass | 6 $GM_\odot$ |
| Elements of the collision | |
| $e$ | 3 |
| $R$ | 10 kpc |
| $i$ | 45° |
| $\omega$ | 90° |
| Viewing parameters | |
| Time | 350 Myr |
| $\lambda$ | 82°5 |
| $\beta$ | 87°5 |

both the body and tidal appendages. The test particles revolve around a central potential which varies radially to simulate a Brandt rotation curve. The Brandt curve parameters, $R_{\max} = 2.9$ kpc and $V_{\max} = 120$ km s$^{-1}$, are the observed parameters of the straight portion of the velocity curve; the exponent $n = 1.84$ in the Brandt formula was chosen such that at the edge of the galaxy a mass of 19 $GM_\odot$ is enclosed. The velocity curve of the system first rises rigidly and then decreases past 2.9 kpc, though not as quickly as for a Keplerian decline. It was found that tidal features are difficult to form if the potential does not decrease at some point. The test particles in the straight portion of the velocity curve were found not to be much disturbed by the passage of the companion.

The sequences of the interaction are displayed in Fig. 11 at intervals of 50 Myr. Two views are shown: normal to the galaxy plane, and from where the galaxy is currently observed. The hyperbolic passage at $i = 45°$, $\omega = 90°$, i.e., slanted with respect to the plane of the galaxy (cf. Fig. 11), together with an eccentricity $e = 3.0$ and a pericenter of $R = 10$ kpc produced enough damage to the galaxy without creating a material bridge of test particles between the two galaxies. The high eccentricity and relatively small pericentric distance were necessary to obtain the observed large radial-velocity difference between the galaxies. The angles $\lambda = 82°.5$ and $\beta = 87°.5$ were selected to produce the observed separation and angle between the two galaxies. The time of viewing is not critical: The galaxy at $T = 300$, 350, and 400 Myr does not look very different. It is interesting to note that material torn out of the galaxy reintegrates with the disk early on.

The different velocity frames of the model at 350 Myr are displayed in Fig. 12. The velocity interval between the frames is 20.673 km s$^{-1}$ as for the original observations. The model reproduces in a satisfactory manner the observed large-scale velocity field of NGC 3448. In particular, the tidal material of the bridge is at lower velocity with respect to the main body, and the tail is found at higher velocity. Final-

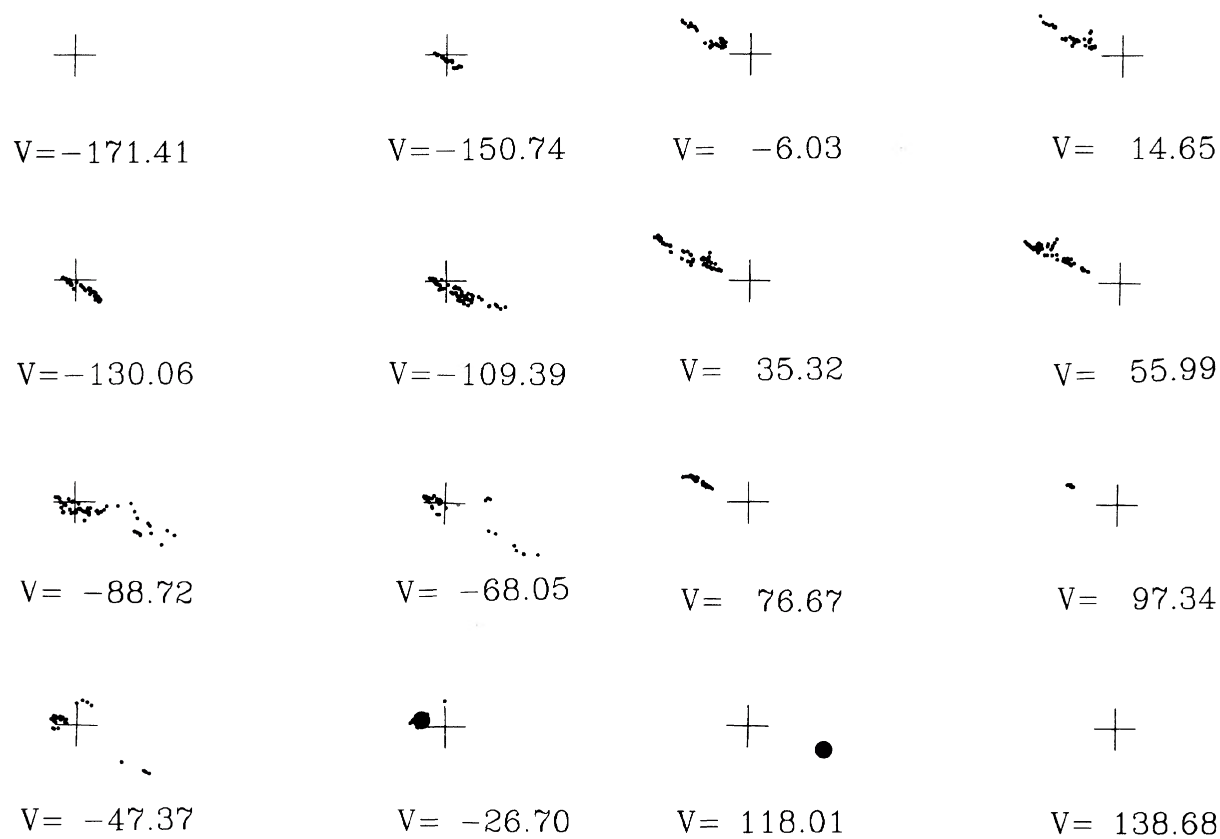


FIG. 12. Velocity frames of the NGC 3448 model. The velocity difference between the frames is 20.673 km s$^{-1}$.

ly, UGC 6016 is found to coincide in position with the bridge of NGC 3448, but with a higher velocity. The only important observational feature not exactly reproduced in the model is the radial-velocity difference between UGC 6016 and NGC 3448, this being too low by about 50 km $s^{-1}$. However, this is not entirely surprising given the limitations of the restricted three-body model mentioned above.

The results of this simulation are illuminating for our understanding of the nature of the double velocity profiles seen in the system, although they are not perfectly reproduced by the model. We suggest that some of this material is foreground to us, is falling toward the galaxy, and will eventually reintegrate with it. This interpretation is supported by the fact that these features coincide with the reddened part of the galaxy.

## V. CONCLUSION

### *a) Summary*

The dynamics of NGC 3448, and Arp 205 as a whole, are uniquely complex. Nevertheless, we are able to generate a model which explains nearly all of the observed features of the H I cube and the optical morphology.

We review the main results of this paper as follows: (1) Dynamically, UGC 6016 is a somewhat normal galaxy, despite being in an interacting pair. (2) The distribution of matter in UGC 6016 is quite regular except for an increase in density in the NE. (3) The mass of UGC 6016 is surprisingly large for a dwarf galaxy, $M_{100''} = 6\ GM_{\odot}$. (4) UGC 6016 is rotating in the opposite sense to NGC 3448, explaining its relatively undisturbed appearance. (5) The two galaxies are not connected by a flow of matter; the "bridge" attached to NGC 3448 is very complex, and only the northern part is visible optically. (6) A new large-scale double profile was discovered using cuts at P. A. = 74°. It is shown to be connected with the previous double velocity profile, and also coincides with reddening in the galaxy. There is combined evidence to show that it is foreground tidal material reintegrating with the galaxy. (7) The H I tail does not coincide exactly with the optical tail, and does not partake in the inner rigid-body rotation. (8) Most of the H I gas in NGC 3448 is in the form of tidal material. (9) The inner part of NGC 3448 rotates like a rigid body. (10) The mass of the inner body of NGC 3448 is $\sim 8.4\ GM_{\odot}$. (11) The three-body interaction model we used was successful in simulating the large-scale structure of NGC 3448.

NGC 3448 is a unique object due to its perturbation by its interaction with UGC 6016. Before the interaction, NGC 3448 was probably a late-type spiral as indicated by its high gas content and the absence of a dominating bulge.

### *b) The Amorphous Phenomenon*

If NGC 3448 were seen from above, it would most probably be classified as a disk galaxy (Fig. 11). This suggests that other amorphous galaxies, especially M82, could be reclassified as normal or slightly peculiar galaxies were they seen from another point of view. The fact that the class of an object depends on the location from which we are observing it is not an unknown phenomenon in galaxy classification.

It is interesting to speculate on the appearance of a galaxy *after* a nonmerging tidal interaction. The matter torn out from the disk or the halo of the galaxy will be stolen by the companion, or it will reintegrate with the "victim" galaxy, or else escape the gravitational attraction of both galaxies. An important question is: Can dynamical friction and kinetic energy dissipation by collisional cooling restore an axisymmetric appearance to the galaxy after a few dynamical times? If so, the amorphous morphology will be temporary.

We are indebted to Jacqueline van Gorkom for her help with observing preparation and data processing at the VLA, and to Bill Schoening and Jeanette Barnes for introducing us to the CCD system at KPNO and the use of the IPPS. We also would like to thank Karl W. Kamper of the David Dunlap Observatory for his help with the use of the PDS densitometer, and M. Duncan for consultation with our dynamical model of NGC 3448. One of us (L.N.) wishes to thank the Fonds F. C. A. C. for Québec-Ontario scholarship. This work was supported by the National Science and Engineering Research Council (NSERC/CRSNG).

## REFERENCES

Arp, H. C. (1966). Astrophys J. Suppl. **14**, 1.

Baars, J. W. M., Genzel, R., Pauliny-Toth, I. I. K., and Witzel, A. (1977). Astron. Astrophys. **61**, 99.

Bertola, F., Casini, C., Bettoni, D., Galletta, G., Noreau, L., and Kronberg, P. P. (1984). Astron. J. **89**, 350.

Borra, E. M., Edwards, G., and Petrucci, F. (1985). Astron. J. **90**, 1529.

Bottinelli, L., Duflot, R., and Gouguenheim, L. (1978). Astron. Astrophys. **63**, 363.

Brandt, J. C. (1960). Astrophys. J. **131**, 293.

Brandt, J. C., and Scheer, L. S. (1965). Astron. J. **70**, 471.

Burstein, D., and Heiles, C. (1984). Astrophys. J. Suppl. **54**, 33.

Combes, F. (1978). Astron. Astrophys. **65**, 47.

Cottrell, G. A. (1977). Mon. Not. R. Astron. Soc. **178**, 577.

Cottrell, G. A. (1978). Mon. Not. R. Astron. Soc. **184**, 259.

D'Addario, L. R. (1982). In *Proceedings of the NRAO-VLA Workshop*, edited by A. R. Thompson and L. R. D'Addario (NRAO, Green Bank), p. 7-1.

Davis, L. E., and Seaquist, E. R. (1983). Astrophys. J. Suppl. **53**, 269.

de Vaucouleurs, G. (1975). In *Stars and Stellar Systems, Vol. 9–Galaxies and the Universe*, edited by A. R. Sandage, M. Sandage, and J. Kristian (University of Chicago, Chicago), p. 578.

de Vaucouleurs, G., de Vaucouleurs, A., and Corwin H. G. (1976). *Second Reference Catalogue of Bright Galaxies* (University of Texas, Austin).

de Vaucouleurs, G., and Pence W. D. (1979). Astrophys. J. Suppl. **39**, 49.

Djorgovski, S. (1984). In *Proceedings of the NASA/SDSU Workshop on Improvements in Photometry*, edited by W. Borucki and A. Young (NASA, Washington, DC), p. 152.

Eichendorf, W., and Nieto, J. L. (1984). Astron. Astrophys. **132**, 342.

Ekers, R. D., and van Gorkom, J. H. (1984). In *Indirect Imaging*, edited by J. A. Roberts (Cambridge University, Cambridge), p. 21.

Faber, S. M., and Gallagher, J. S. (1979). Annu. Rev. Astron. Astrophys. **17**, 135.

Goad, J. W., editor (1981). *Facilities Book* (Kitt Peak National Observatory, Tucson).

Gottesman S. T., and Weliachew, L. (1977). Astrophys. J. **211**, 47.

Hodge, P. W. (1966). Astrophys. J. **146**, 593.

Huchra, J. P., and Geller, M. J. (1982). Astrophys. J. **257**, 423.

Huchtmeier, W. K., and Bohnenstengel, H. D. (1975). Astron. J. **44**, 479.

Killian, D. J., and Gottesman, S. T. (1979). In *Photometry, Kinematics, and Dynamics of Galaxies*, edited by D. S. Evans (University of Texas, Austin), p. 267.

Kronberg, P. P., Biermann, P., and Schwab, F. R. (1981). Astrophys. J. **246**, 751.

Lake, G., and Schommer, R. A. (1984). Astrophys. J. Lett. **279**, L19.

Larson, R. B., and Tinsley, B. M. (1978). Astrophys. J. **219**, 46.
Lequeux, J. (1983). Astron. Astrophys. **125**, 394.
Lewis, B. M., and Davies, R. D. (1973). Mon. Not. R. Astron. Soc. **165**, 213.
Longo, G., and de Vaucouleurs, A. (1983). *A General Catalog of Photometric Magnitudes and Colors in the U, B, V System of 3578Galaxies Brighter than the 16th Magnitude, 1936–1982* (University of Texas, Austin).
McGuire, T. E. (1983). Publ. Astron. Soc. Pac. **95**, 919.
Nordsieck, K. H. (1973). Astrophys. J. **184**, 719.
Noreau, L. (1985). Ph.D. thesis, University of Toronto.
Noreau, L., and Kronberg, P. P. (1986). In preparation.
Nilson, P. (1973). *Uppsala General Catalog of Galaxies*, Uppsala Obs. Ann. **6**.
O'Connell, R. W., and Mangano, J. J. (1978). Astrophys. J. **221**, 62.
Peterson, S. D., and Shostak, G. S. (1974). Astron. J. **79**, 767.
Reakes, M. (1979). Mon. Not. R. Astron. Soc. **187**, 509.
Rickard, L. J, Palmer, P., Morris, M., Zuckerman, B., and Turner, B. E. (1975). Astrophys. J. Lett. **199**, L75.
Roberts, M. S. (1972). In *External Galaxies and Quasi-Stellar Objects*, IAU Symposium No. 44, edited by D. S. Evans, D. Wills, and B. J. Wills (Reidel, Dordrecht), p. 12.
Rots, A. H. (1982). In *Proceedings of the NRAO-VLA Workshop*, edited by A. R. Thompson and L. R. D'Addario (NRAO, Green Bank), p. 8-1.
Rots, A. H. (1983). *A Short Guide for VLA Spectral Observers* (NRAO, Green Bank).
Sancisi, R., and Allen, R. J. (1979). Astron. Astrophys. **74**, 73.
Sandage, A. R., and Brucato, R. (1979). Astron. J. **84**, 472.
Sandage, A. R., and Tammann, G. A. (1981). *A Revised Shapley-Ames Catalog of Bright Galaxies* (Carnegie Institution of Washington, Washington, DC).
Schoening, W. (1983). *Operation of the CCD Direct-Imaging Camera For The #1 0.9 Meter Telescope, Kitt Peak National Observatory* (Kitt Peak National Observatory, Tucson).
Schweitzer, F. (1976). Astrophys. J. Suppl. **31**, 313.
Smithsonian Astrophysical Observatory Star Catalog (1966). (U. S. GPO, Washington, DC).
Sydserff, P., and Cruise W. (1985). Bull. Inf. CFHT No. 12, 3.
Tammann, G. A. (1980). In *Dwarf Galaxies*, edited by M. Tarenghi and K. Kjar (European Southern Observatory, Munich), p. 2.
Telesco, C. M., and Harper, D. A. (1980). Astrophys. J. **235**, 392.
Thompson, A. R., Clark, B. G., Wade, C. M., and Napier, J. P. (1980). Astrophys. J. Suppl. **44**, 151.
Toomre, A., and Toomre, J. (1972). Astrophys. J. **178**, 623.
Tully, R. B. (1982). Astrophys. J. **257**, 389.
Tully, R. B., Bottinelli, L., Fisher, J. R., Gouguenheim, L., Sancini, R., and van Worden, H. (1978). Astron. Astrophys. **63**, 37.
Turner, E. L., and Gott, J. R. (1976). Astrophys. J. Suppl. **32**, 409.
van den Bergh, S. (1959). Publ. David Dunlap Obs. **2**, No. 5.
van der Hulst, J. M. (1979). Astron. Astrophys. **75**, 97.
van Gorkom, J. H. (1982). In *Proceedings of the NRAO-VLA Workshop*, edited by A. R. Thompson and L. R. D'Addario (NRAO, Green Bank), p. 15-1.
Warner, P. J., Wright, M. C. H., and Baldwin, J. E. (1973). Mon. Not. R. Astron. Soc. **163**, 163.
Weliachew, L., Sancisi, R., and Guelin, M. (1978). Astron. Astrophys. **65**, 37.
Wright, M. C. H. (1974). In *Galactic and Extra-Galactic Radio Astronomy*, edited by G. L. Verschuur and K. I. Kellermann (Springer, New York), p. 291.